Experimental characterization and numerical modeling of the porosity formation mechanisms in thermoplastic laminates at high temperature

David Philippe, Benoit Vieille, Fabrice Barbe

▶ **To cite this version:**

David Philippe, Benoit Vieille, Fabrice Barbe. Experimental characterization and numerical modeling of the porosity formation mechanisms in thermoplastic laminates at high temperature. Springer Proceedings in Mathematics & Statistics, inPress. hal-04523950

HAL Id: hal-04523950
https://hal.science/hal-04523950

Submitted on 27 Mar 2024

HAL is a multi-disciplinary open access archive for the deposit and dissemination of scientific research documents, whether they are published or not. The documents may come from teaching and research institutions in France or abroad, or from public or private research centers.

L'archive ouverte pluridisciplinaire **HAL**, est destinée au dépôt et à la diffusion de documents scientifiques de niveau recherche, publiés ou non, émanant des établissements d'enseignement et de recherche français ou étrangers, des laboratoires publics ou privés.

Experimental characterization and numerical modeling of the porosity formation mechanisms in thermoplastic laminates at high temperature

David Philippe[0000−0003−4748−9715],
Benoit Vieille[0000−0003−4528−7167] and
Fabrice Barbe[0000−0001−5819−1696]

Abstract Subjecting thermoplastic-based laminates to high thermal energy, such as a flame, leads to the gradual deterioration of the matrix, involving solid-state changes and significant fluctuations in thermomechanical properties. Despite these changes and the presence of substantial temperature gradients, the laminates can still bear mechanical loads, even after the matrix has melted. When temperatures exceed the melting point, the primary mechanism of matrix thermal decomposition involves the formation of voids. While these voids weaken the material from a mechanical perspective, they also act as thermal insulators, protecting the matrix on the side facing away from the heat source. To accurately describe the evolution of thermomechanical properties whereas one face of the laminates is exposed to a flame, it is crucial to understand the kinetics of void formation. Experimental investigations revealed that porosity content and swelling are strongly dependent on the time and temperature of thermal exposure. A mesoscopic Finite Element model was thus developed, representing porosities at a structural level. The formation of voids and the associated swelling were simulated using a probabilistic approach, guiding the progressive transformation of elements into voids based on their thermal state.

David Philippe
Groupe de Physique des Matériaux, CNRS, Normandie Univ., Univ. Rouen, INSA Rouen, 76000 Rouen, France, e-mail: david.philippe@insa-rouen.fr

Benoit Vieille
Groupe de Physique des Matériaux, CNRS, Normandie Univ., Univ. Rouen, INSA Rouen, 76000 Rouen, France e-mail: benoit.vieille@insa-rouen.fr

Fabrice Barbe
Groupe de Physique des Matériaux, CNRS, Normandie Univ., Univ. Rouen, INSA Rouen, 76000 Rouen, France e-mail: fabrice.barbe@insa-rouen.fr

1 Introduction

This work discusses the challenges faced by aeronautical structural parts made from polymer matrix composite materials when exposed to high thermal energy conditions. These conditions can range from ambient temperature to the temperature at which the polymer starts to decompose (around 450°C). The ability of the composite to withstand these conditions depends on the degradation of its constituent properties, particularly the polymer matrix. To understand the mechanics and thermal transfers in such scenarios, a combination of experimental and numerical analyses is required to replicate critical operating conditions like fires in aircraft engines.

In the continuation of previous works [1, 2, 3], this study focuses on the behavior of a specific composite material, Quasi-Isotropic Carbon fiber reinforced PolyPhenylene Sulfide (QI C/PPS) laminates, as they are exposed to heat. It discusses how various changes occur in the material, particularly in the polymer matrix, due to temperature fluctuations. Whereas the carbon fiber thermomechanical behavior remains almost temperature independent below 700°C [4], the thermoplastic polymer matrix undergoes state transitions at different temperatures: glassy at ∼90°C, melting at ∼270°C and then thermal decomposition at ∼450°C, above which pyrolysis takes place [5, 6, 7]. As a consequence, in the context of a directional thermal aggression such as a flame, high thermal gradients will take place, involving the different solid-state transformations of the matrix; it leads in particular to the formation of cavities which although they weaken the mechanical properties act as a thermal insulator for the polymer matrix away from the flame. Accurate descriptions and models of the material's thermomechanical behavior in this context need to consider time and temperature dependencies, as well as the heterogeneous nature of the composite's meso-structure, including the local porosity content.

To reach these objectives, this study first proposes an experimental characterization of the porosity formation in order to identify and quantify the various involved mechanisms: nucleation and growth of porosities in the polymer matrix zones, fiber bundle / matrix interface debonding, intra-fiber bundle porosity formation, and the accompanying mechanism of cavity pressurization (due to pyrolysis gas) leading to swelling on the laminates macroscale. The results are then used as inputs for the development of a numerical model reproducing the temperature dependent phenomenon of porosity formation on the local scale of the laminates. The kinetics of porosity formation during the thermal decomposition of the matrix has been widely covered experimentally using mass loss measurements [8, 9, 7, 10, 11]. Analytical laws have been found to numerically reproduce this kinetics [12, 13, 14, 1]. However, these approaches only consider the porosity content as a variable of the numerical model, while an explicit representation of the porosity distribution is required to accurately take into account their influence on the laminates behavior [15, 1, 16]. The proposed numerical approach consists in explicitely representing the biphase meso-structure of the laminates (woven fiber bundles and matrix) and in explicitely introducing the nucleation and growth of porosities from a temperature and time dependent kinetics law identified from the experiments. Various possibilities to be examined in future studies are presented to account for the experimental results regarding the fiber bundle / matrix interface debonding and the intra-fiber bundle porosities.

2 Porosity formation mechanisms

During the exposure to a temperature above that of polymer matrix decomposition, porosities gradually form within the material, with a macroscale kinetics law significantly depending on time and temperature [3]. To have a view on the corresponding porosity network on the local scale of the laminates, Fig. 1a presents a 3D representation, as obtained from X-Ray tomography analysis, of the porosities distribution after 5 minutes of isothermal treatment at 530°C. A 2D representation is provided in Fig. 1b: a 2D plane at half thickness of the laminates (i.e. a plane parallel to the plate of the laminates) has been extracted and segmentation was set such as to show only the polymer and the porosities. The XRay tomography and optical microscopy analyses of samples isothermally decomposed for different temperatures and times (see Ref. [3]) have enabled to draw up a classification of the porosities according to four main categories:

- 1: Small circular porosities which have just nucleated

- 2: Intermediate circular porosities which have grown/coalesced
- 3: Large macro-porosites which originate (at least partly) from the interface debonding
- 4: Intra-fiber bundle porosities whose shape are mainly longitudinal along the fiber direction

It is to be noted that, until they reach a certain size, the porosities located in the matrix-rich areas appear to have a spherical shape, as expected from gas bubbles forming within melted polymer. However, the growth and coalescence processes are not entirely understood, as well as their interaction with the delamination. Is there a minimum/maximum size for a nucleated porosity? Does it occur instantaneously and is followed by the growth? How does the external surface of the porosities exactly grow, or does it consist in a coalescence of many smaller pockets? Hence, the exact contribution of all three porosity formation mechanisms is not yet fully explained.

(a) (b)

Fig. 1: X-Ray tomography observations of a laminates sample after 5 minutes exposure at 530°C: (a) extracted porosities in 3D of a $4.3 \times 4.3 \times 2.21\text{mm}^3$ domain, (b) porosities (in red) and matrix (in grey) in a 2D slice at half thickness. Numbers 1 to 4 refer to the proposed classification of porosities.

The evolution of the porosity content in C/PPS QI laminates with temperature has been established in previous works [3] (Fig. 2), along with the thickness expansion resulting from the porosity formation (Fig. 3). The following sections describe the experimental study and numerical modeling carried out on the four porosity formation mechanisms aforementioned i.e. nucleation and growth of porosities within the matrix, fiber bundle / matrix interface debonding and intra-fiber bundle porosities. The porosity content resulting from the experimental tests (on $25 \times 25 \times 2.21\text{mm}^3$ samples) has been used as input for the finite element numerical modeling at a mesoscopic scale (Fig.4).

3 Modeling based on nucleation only

The nucleation modeling is extensively described in [3]. The transformation of matrix elements into porosity ones relies on a probability depending on time and temperature. Let us note η_p the porosity content in the laminates (i.e. the volume fraction of porosities), Δt the time increment of a finite element calculation and $p\left(t, T, \Delta t\right)$ the probability of a matrix element to transform into a porosity within the time Δt. The kinetics law of the porosity formation reads:

$$\begin{aligned} &\dot{\eta}_p\left(t,T\right) = G_N\left(t,T\right)\left(1-\eta_p\left(t,T\right)\right) \qquad \forall t \geq 0,\ \forall T \geq T_\text{d} \\ &\text{where} \quad G_N\left(t,T\right) = \frac{p\left(t,T,\Delta t\right)}{\Delta t} \end{aligned} \tag{1}$$

$G_N\left(t,T\right)$ is the rate function enabling to control the kinetics of porosity formation in the specific case where porosities only form by nucleation. As to enable the identification of $G_N\left(t,T\right)$ from macroscale measurements of $\eta_p(t,T)$ in a large spectrum of temperatures and times, a phenomenological form of $G_N\left(t,T\right)$ was chosen, as expressed in 2, calling upon parameters having separate effects on $\eta_p(t,T)$.

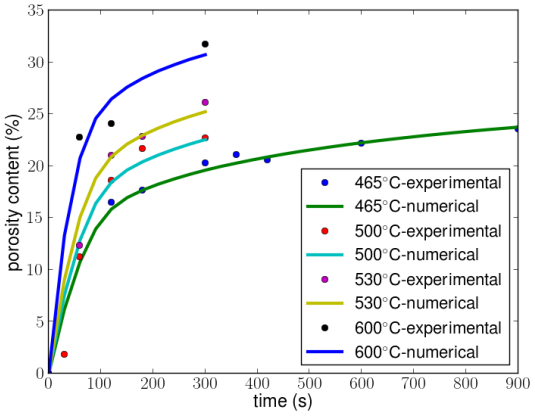

Fig. 2: Comparison of the experimental / numerical evolution over time of the porosity content η_p (volume fraction of porosities) for different temperatures of exposure. The numerical results correspond to the model accounting only for the nucleation mechanism, extracted from [3].

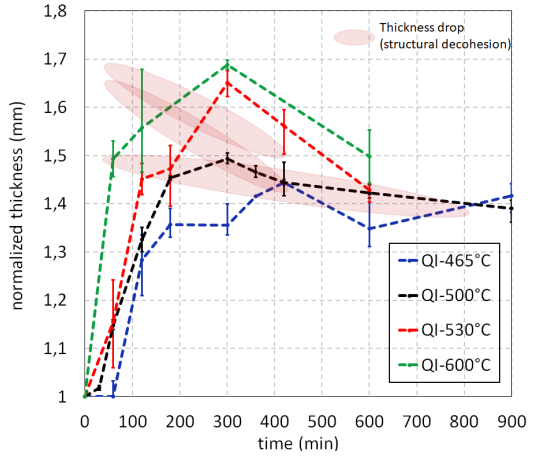

Fig. 3: Evolution over time of the laminates thickness for different temperatures of exposure, extracted from [3]

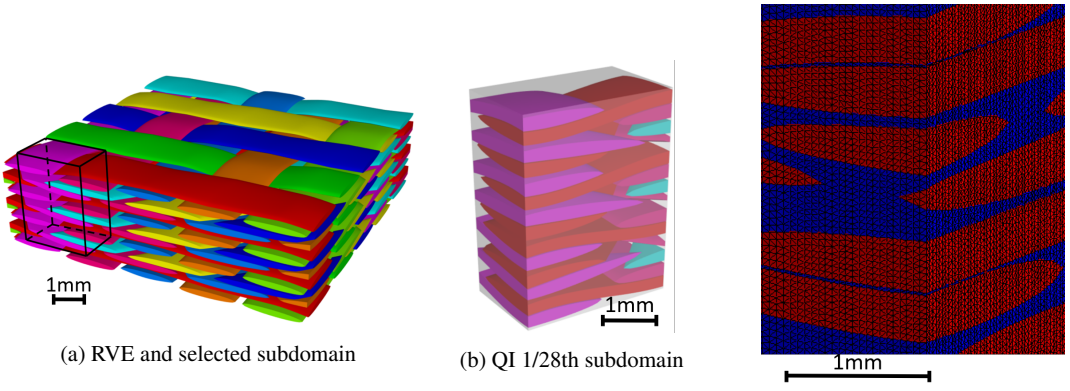

(a) RVE and selected subdomain

(b) QI 1/28th subdomain

(c) Zoom on the subdomain mesh

Fig. 4: 3D mesoscopic numerical model of the laminates. Colors are used to differentiate the fiber bundles [3]

$$G_N(t,T) = \frac{a_1 + a_2\left(\frac{T - T_d}{T^{ref} - T_d}\right)^b}{t + \tau} \tag{2}$$

The five parameters of $G_N(t,T)$ have been identified by an optimization process where, at each iteration, the integration of Eq. 1 from the Euler's method is compared to the considered reference experimental $\eta_p(t,T)$. Fig. 2 shows that the numerical model accurately reproduces the experimental porosity formation kinetics for various temperatures of exposure. A limitation is observed for the highest temperatures due to experimental uncertainties as explained in [3].

4 Modeling based on nucleation and growth

4.1 Principles of the modeling

As X-Ray tomography observations have shown, cavities can be present in the form of small or large voids. These latter case are obtained from the mechanism of growth. To introduce this mechanism in the modeling, it has been chosen to assign to each element of polymer matrix a supplementary probability of transforming into cavity which depends on its location with respect to existing cavities (or nuclei) following this principle: given a distribution of nuclei and the relative field of porosity density, the larger the porosity density in the surrounding of the considered element, the larger the probability to transform into a cavity.
Let $p_{growth}(t,T,\Delta t)$ be this probability at time t, temperature T and during the time increment Δt. The total probability of an element to transform into a cavity is then defined by Eq. 3.

$$p(t,T,\Delta t) = p_{\text{nucleation}}(t,T,\Delta t) + p_{\text{growth}}(t,T,\Delta t) \tag{3}$$

p_{growth} at a given matrix element is determined from the density of porosities in its direct neighborhood. Let a domain occupied by matrix element be divided into cubic *boxes* where the local porosity densities are computed. As represented in Fig. 5, each box contains of the order of few matrix elements and three scales are considered to determine the probability of transformation of an element:

- Scale of an element: matrix/porosity finite element of the model
- Scale of a *box*: it contains a fixed number of matrix elements defining its size. The example provided in this section considers 5 elements in each box. A difference is made between the box of interest containing the matrix element and the surrounding boxes.
- Scale of a *local domain*: ensemble of boxes surrounding a given matrix element

The boxes constituting a *local domain* are classified according to their distance from the central box: the 1^{st} order is the box of interest, the 2^{nd} order ones are the 26 boxes in the direct neighborhood, the 3^{rd} order ones are the next 37, etc. The effect of the neighborhood of a given element on its transformation probability is maximum for the elements located inside the box of interest and decreases as the order of classification increases.

Let us note n the number defining the classification order of neighbours and d_i the porosity density in the boxes i forming the local domain of a given matrix element. The probability of transformation of an element inside the box of interest is determined from a weighted average of the porosity densities in the local domain according to Eq. 4, where ω_i stand for the weight constants for $i \in \left[3^{k-1}+1, 3^k\right]$, $k \in \{1, ..., n\}$.

$$p_{\text{growth}} = \sum_{i=1}^{3^n} \omega_i d_i \tag{4}$$

The weight constants $(\omega_i)_{i\in\left[3^{k-1}+1,3^k\right],k\in\{1,....,n\}}$ then constitute the set of parameters governing the kinetics of growth. The form they have been given in order to introduce the dependence of the growth rate to temperature and time, and the identification that could be made from the experimental results of porosity content evolution through time for the different temperatures of exposure are presented in section 4.4.

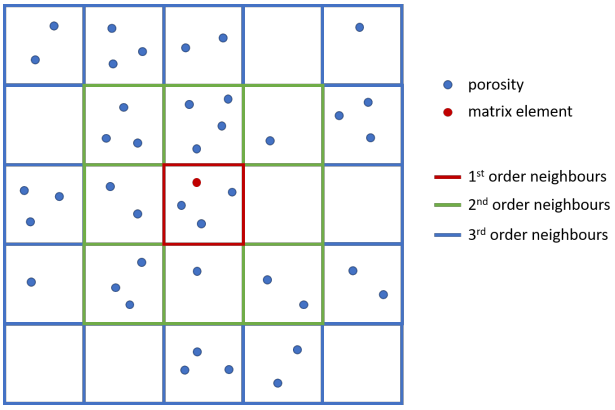

Fig. 5: 2D representation of the *local domain* around a given *box* of interest and the associated classification of the neighborhood from 1^{st} to 3^{rd} order.

In order to illustrate how this model works, let us consider the case where a box contains five elements, being either matrix or porosity, and $n = 2$, as depicted in 2D in Fig. 6, along with the corresponding densities of the constituent boxes of the local domain.

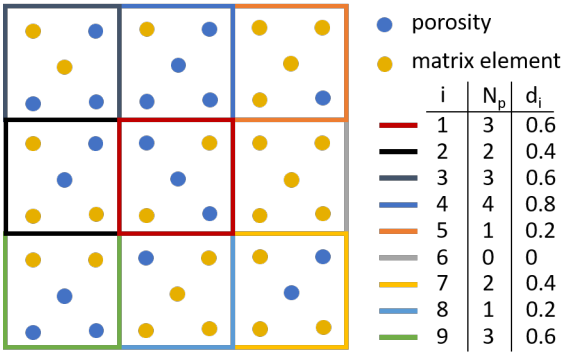

i	N_p	d_i
1	3	0.6
2	2	0.4
3	3	0.6
4	4	0.8
5	1	0.2
6	0	0
7	2	0.4
8	1	0.2
9	3	0.6

Fig. 6: 2D illustration of the porosity distribution within the boxes of a 2*nd* order local domain considering a box size of 5 elements. Calculation of the porosity density of the boxes forming the local domain

Let us assume further that $\omega_1 = 0.2$ and $\omega_{2,\dots,9} = 0.1$. Eq 4 then gives a probability of transformation in the central box of interest $p_{\text{growth}} = 0.38$.

4.2 Strategy for the application in a FE thermomechanical computation

The question first rests on the compromise between the maximum order of influence considered and the amount of elements placed in each box. These considerations must rely on a reasonable computation time while preserving the chemico-physical aspect of the phenomenon:

- On the one hand, an ideal system would consist in considering each box containing only one matrix element influenced by the other elements directly connected to it. It is however not numerically feasible. On the other hand, an extremely cost effective discretization considering too many elements in each box would not be representative enough.
- Taking into account too many orders would result in (i) large calculation times and (ii) loss of accuracy as elements would interact from a large distance.

As a first approach in the present work, the following configuration was chosen:

- Only 1st and 2nd order neighbors, which results in a local domain made of the central box and its 26 neighbors,
- 10 elements in each box, which corresponds to 2 to 3 elements along each direction of space within a box, and which is also an appropriate number of almost identical tetrahedra for filling a cube without voids; this consideration makes sense as regard the tetrahedral elements used for meshing the laminates.

4.3 Comparison with JMAK

The JMAK model (Johnson-Mehl-Avrami-Kolmogorov) provides a reference kinetics law of the macroscale porosity content since it relies also on the mechanisms of nucleation and growth of a product phase within a parent one. From the instantaneous initial nucleation of a certain nuclei volume fraction $z\,(t=0)$, and given an isotropic and time-independent growth rate, the rate of transformation to the product phase can be integrated in the form of Eq. 5, where $z\,(t)$ (assimilated to $\eta_p\,(t)$) stands for the volume fraction of the product phase:

$$z\,(t) = 1 - exp\,(-Kt^n) \tag{5}$$

K is a constant depending on $z\,(t=0)$ and the interface growth velocity.
n is an integer no larger than 4, usually set at $D+1$, D being the dimension of the geometrical model. In the present case, $n=4$ since our model is three-dimensional.

Let us set as an example $z\,(t=0) = 0.1\%$ in the numerical model and $K = 1.3E-9$. Let us suppose that the nucleation only occurs at the initial time in the proposed finite element growth model so that only the growth governs the porosity content evolution. A cubic domain of matrix containing 1,000,000 elements was used. It was found that the weights of the present approach (as described in Eq. 6) can be adjusted as to fit the JMAK-predicted evolution (Fig. 7). This shows that the proposed numerical growth model, although established on a local scale, has the capacity to reproduce JMAK-like macroscale kinetics.

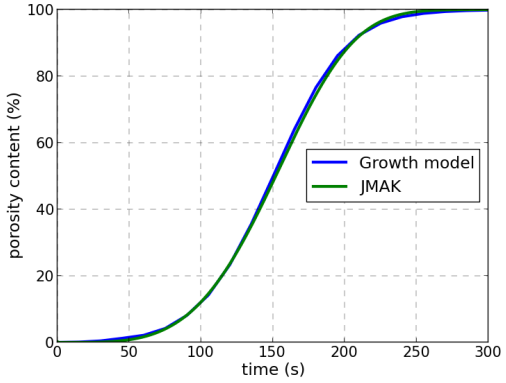

Fig. 7: Comparison of the porosity content evolution over time as obtained by the JMAK model and the nucleation-and-growth model ($\eta_p\,(t=0) = 0.1\%$).

4.4 Growth model identification

In the modeling of porosity formation from nucleation and growth, $G_N\,(t,T)$ must be lowered with respect to its identification in the modeling based only on nucleation. In the case of exposure where porosities form large pockets (high temperature and rather long time of exposure), the porosity formation can be assumed

to be governed by the growth mechanism. To address this situation, as a first approach to demonstrate the capabilities of the growth model, the nucleation probability was arbitrarily divided by 2.5 so that 40% of the porosity content corresponds to nuclei and 60% originate from the growth.

As mentioned in Section 4.1, it is necessary to account for the second order neighbors for the welfare of the modeling. However their influence (or weight) can be reduced to a minimum. To that end, it was chosen arbitrarily to set the weight of the central box 80 times higher than the surrounding ones. Doing that, the combined weight of the 26 surrounding boxes is around 3 times lower and represents 25% of the total weight.
As for the determination of G_N, the weights ω_i must follow a similar trend: a high value at the initial times to initiate the growth process, before decreasing with time. The proposed definition of ω_i reads:

$$\omega_i\left(t,T\right) = \frac{1}{\left(\tau_{1,i} + \tau_{2,i}\left(\frac{T - T_d}{T_{\text{ref}} - T_d}\right)\right) t^c} \qquad \text{with t>0} \tag{6}$$

As the growth occurs after the nucleation and the first iteration is at the end of the first time step of the finite element calculation, $t > 0$. The various parameters and their roles are presented in Table 1.

Parameter	Unit	Value		Main role
		$i = 1$	$i = \{2...9\}$	
τ_1	Time (s)	$1.37e-4$	$1.09e-2$	Affects ω_i for $T = T_{\text{ref}}$
τ_2	Time (s)	$5.77e-6$	$4.62e-4$	Dependence of ω_i to T
c	No unit	2.2	2.2	Non-linear dependence of ω_i to t
T_{ref}	Temperature (°C)	530	530	Reference temperature

Table 1: Parameters used to define $\omega_i\left(t,T\right)$ as given by Eq. 6

The parameters from the definition $\omega_i\left(t,T\right)$ were identified in order to fit the experimental data, and the obtained porosity content evolution is depicted on Fig. 8. It appears that the optimized parameters accurately replicate the experimental results similarly to what has been obtained with the model based only on nucleation, along with the same uncertainties for the highest temperature level.

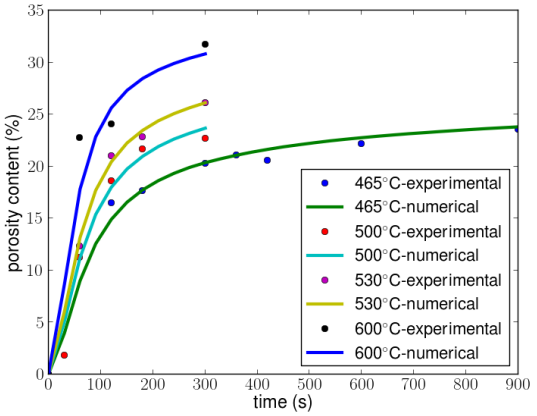

Fig. 8: Comparison of the experimental / numerical evolutions over time of η_p for different temperatures of exposure considering the model based on nucleation and growth.

4.5 Nucleation based *vs* Nucleation-and-growth based modeling

As shown in sections 3 and 4.4, could it be by nucleation only or by nucleation and growth, both mechanisms enable to reproduce correctly the evolution of the porosity content through time for the different tested temperatures of exposure. But these models intrisically lead to different morphologies of cavities, as can be seen on Fig. 9. It presents the distribution of finite elements of porosities in a cubic mesh domain constituted of matrix only, where 54% of porosities have been generated from each model for a given isothermal exposure. Whereas porosities are uniformally distributed with the nucleation model, the nucleation-and-growth model leads to large clusters of porosities embedded within large matrix areas as well.

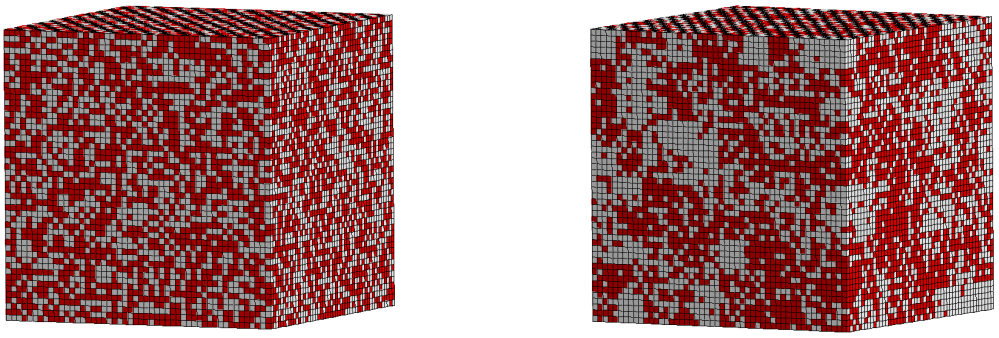

(a) (b)

Fig. 9: Porosity distribution (in red) for a 54% porosity content in a domain of matrix elements (100%): (a) nucleation only, (b) with an initial nucleation of 25% porosities then growth

Another way to highlight the difference in the spatial distribution of porosities from a model to the other is provided by the statistical distributions of the local porosity density (or porosity volume fraction). Fig. 10 presents these distributions at different instants of an isothermal exposure. Whereas the nucleation-based model produces -evidently- normal distributions translating to high values of the porosity volume fraction as time of exposure increases, keeping a constant standard deviation, the nucleation-and-growth model leads to distribution which evolve through time in terms of shape, average value and standard deviation. The most important change in the distribution is observed at the earliest steps of the porosity formation.

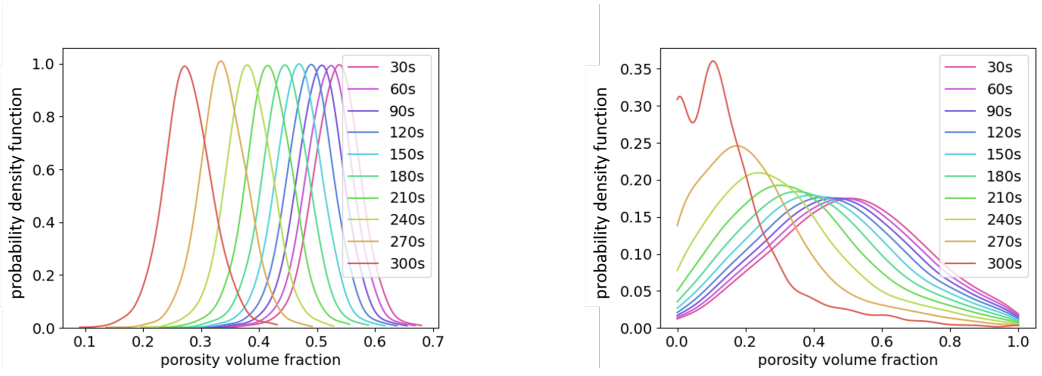

(a) (b)

Fig. 10: Evolution through time of the distribution of the porosity density in each box over time. Porosities formed through (a) nucleation, (b) nucleation and growth

5 Towards a comprehensive modeling of the porosity formation

The identification of the numerical models accounting for nucleation-only or for nucleation-and-growth have been established with respect to the experimental measurements of the porositiy content evolutions. No conclusive model has yet been developed to reproduce the fiber bundle / matrix interface debonding and the intra-fiber bundle porosity. This section presents the preliminary experimental tests which have been carried out to quantify these phenomena.

5.1 Fiber bundle / matrix interface debonding

Generally, under thermal aggression, the mechanism of debonding at the interface between a fiber bundle and the matrix first takes place at the interface between plies because this is where most of the porosities resulting from the processing of the material are present [17, 18].

Fig. 3 presents the thickness expansion through time for different temperatures of exposure. For some of the samples characterized, the thickness expansion was originating from both the pressurization of the pyrolysis gas within the porosities and interface debonding. These two phenomena thus need to be differentiated as to how they influence the swelling of the laminates.
In order to quantify the role of each mechanism, laminates samples have been exposed to temperatures in the range from 250°C to 450°C. It was indeed observed that interface debonding can occur for temperatures lower than that of the thermal decomposition (as can be seen on Fig. 11 at 350°C).

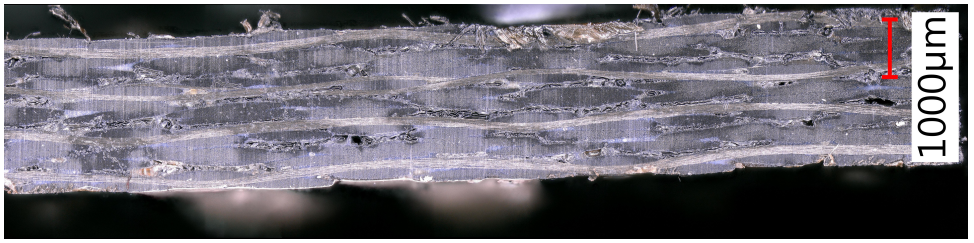

Fig. 11: Optical microscope observation of the porosities resulting from the debonding of C/PPS laminates after 5min of thermal exposure at 350°C

The same protocol as the one used in [3] has been followed using a furnace and three samples for each time/temperature conditions. The interface decohesion can then be isolated and the trend of its evolution over time and temperature determined. The obtained trend was then assumed to stay similar throughout the decomposition process. As a result, the thickness expansion originating from the interface debonding was obtained for the whole range of temperatures $[250; 600]$ °C, and the one resulting from the pressurization was directly deduced. The experimental results of this method is presented on Fig. 12 for various times of exposure. The debonding-related expansion was found to have a converging tendency, while a clear increase was observed at the onset of the thermal decomposition. Although no numerical modeling of the debonding has been performed, cohesive elements could be used in future works to reproduce this mechanism.

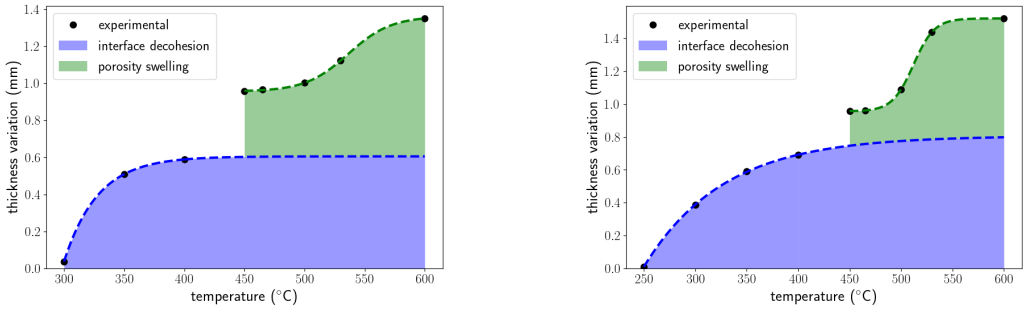

Fig. 12: Evolution of the thickness expansion over time, differentiating the pressurization and debonding mechanisms after (a) 3 minutes, (b) 5 minutes of exposure

5.2 Intra-fiber bundle porosity

In order to accurately model the thermomechanical behavior of a laminates in future works, it is necessary to account for the porosity formation within the fiber bundles. Indeed, it will reduce the mechanical loading capacity through (i) matrix being replaced by voids and (ii) lowering of the fiber cohesion which is maintained by the matrix.

The porosity content within the fiber bundles has been determined from 2D optical microscope observations extracted from the core of the samples. A grey scale threshold has been used. The results presented in Fig. 13 show the progressive increase of the porosity content over time and temperature. One can note in particular that the total amount of porosities within a fiber bundle reaches 20 to 25% of the total volume of matrix in the fiber bundle.

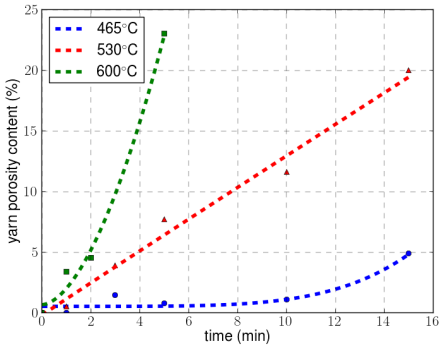

Fig. 13: Evolution of the porosity content inside the fiber bundles over time for different temperatures in C/PPS QI laminates, as measured from optical microscopy scans. The measured porosity content is related to the total amount of matrix within a fiber bundle.

To include this mechanism in the modeling remains an open question. From the point of view of the thermal problem, it might be sufficient to approximate the fiber bundle conductivity from a mixture rule or from an homogenization scheme. From the mechanical point of view, in Ref. [19] it is proposed to directly relate the mechanical properties of the fiber bundle to the porosity content, as in the classical theory of the damage of materials. The relevance of such an approach is however questionable: yet it might lead to a rather correct approximation concerning the axial stiffness of a fiber bundle, its accuracy concerning the shear modulus of the fiber bundle is called into question since the porosities are distributed according to a

network aligned in the direction of the fibers. The development of a solution to account for this mechanism in the modeling will be the subject of future works.

6 Conclusion

In the context of one-sided exposure to high thermal energy sources like flames, the tensile strength of polymer matrix composite laminates decreases significantly, but it remains substantial for a considerable duration, preventing catastrophic failure. A key factor in this degradation is the pyrolysis of the matrix. This article takes part to a series of modeling developments for the progressive thermal decomposition of the polymer matrix within a composite laminate, focusing on: (1) Describing thermal gradients accurately, (2) Modeling the kinetics of porosity formation during matrix decomposition to account for the rapid evolution of the polymer state, (3) Explicitly representing the presence of voids that act as thermal insulators, (4) Developing a model allowing the thermomechanical coupling to be simulated. Its first originality lies in the extension of a previous model (in [3], accounting only for the nucleation of cavities, to the mechanism of growth of cavities. Along with these new developments, based on X-Ray tomography and optical microscopy analyses, the principal mechanisms driving the formation of porosities and the swelling of the laminate have been differentiated: nucleation and growth inside the matrix rich regions, debonding at the interface between a fiber bundle and the matrix, intra-fiber bundle porosity formation. Possible methodologies to include the mechanisms of debonding and intra-bundle porosity formation are discussed, paving the ground for future developments.

References

1. Y. Carpier, B. Vieille, A. Coppalle, F. Barbe, Polymer Composites **41**(9), 3552 (2020). DOI https://doi.org/10.1002/pc.25641
2. Y. Carpier, A. Alia, B. Vieille, F. Barbe, Polymer Degradation and Stability **186**, 109525 (2021). DOI https://doi.org/10.1016/j.polymdegradstab.2021.109525
3. D. Philippe, B. Vieille, F. Barbe, Composites Part B: Engineering **266**, 111026 (2023). DOI https://doi.org/10.1016/j.compositesb.2023.111026. URL https://www.sciencedirect.com/science/article/pii/S1359836823005292
4. S. Feih, A. Mouritz, Composites Part A: Applied Science and Manufacturing **43**(5), 765 (2012). DOI https://doi.org/10.1016/j.compositesa.2011.06.016. Office of Naval Research (ONR): Composites in Fire
5. J. Bibinger, S. Eibl, H.J. Gudladt, Applied Composite Materials **29**(5), 1817 (2022)
6. T.M. Vetter, S. Eibl, H.J. Gudladt, Applied Composite Materials **28**(2), 427 (2021)
7. C.C.M. Ma, H.C. Hsia, W.L. Liu, J.T. Hu, Journal of Thermoplastic Composite Materials **1**(1), 39 (1988). DOI 10.1177/089270578800100104
8. S.C. Moldoveanu, in *Analytical Pyrolysis of Synthetic Organic Polymers*, *Techniques and Instrumentation in Analytical Chemistry*, vol. 25 (Elsevier, 2005), pp. 31–107. DOI https://doi.org/10.1016/S0167-9244(05)80003-4
9. F. Yao, J. Zheng, M. Qi, W. Wang, Z. Qi, Thermochimica Acta **183**, 91 (1991). DOI https://doi.org/10.1016/0040-6031(91)80448-R
10. P. Patel, T.R. Hull, R.E. Lyon, S.I. Stoliarov, R.N. Walters, S. Crowley, N. Safronava, Polymer Degradation and Stability **96**(1), 12 (2011). DOI https://doi.org/10.1016/j.polymdegradstab.2010.11.009
11. G.F. Levchik, K. Si, S.V. Levchik, G. Camino, C.A. Wilkie, Polymer Degradation and Stability **65**(3), 395 (1999). DOI https://doi.org/10.1016/S0141-3910(99)00028-2
12. M. Day, D. Budgell, Thermochimica Acta **203**, 465 (1992). DOI https://doi.org/10.1016/0040-6031(92)85217-J
13. M. Starink, Thermochimica Acta **404**(1), 163 (2003). DOI https://doi.org/10.1016/S0040-6031(03)00144-8
14. W. Endres, M.D. Lechner, R. Steinberger, Macromolecular Materials and Engineering **288**(6), 525 – 530 (2003). DOI 10.1002/mame.200390050. Cited by: 18
15. A. Mouritz, A.G. Gibson, *Fire Properties of Polymer Composite Materials*, *Solid Mechanics and Its Applications*, vol. 143 (Springer, 2006). DOI https://doi.org/10.1007/978-1-4020-5356-6
16. Y. Carpier, B. Vieille, F. Barbe, A. Coppalle, Composites Part A: Applied Science and Manufacturing **162**, 107165 (2022). DOI https://doi.org/10.1016/j.compositesa.2022.107165
17. L. Amedewovo, A. Levy, B. de Parscau du Plessix, J. Aubril, A. Arrive, L. Orgéas, S. Le Corre, Composites Part A: Applied Science and Manufacturing **167**, 107412 (2023). DOI https://doi.org/10.1016/j.compositesa.2022.107412. URL https://www.sciencedirect.com/science/article/pii/S1359835X22005930
18. S. Sihn, J. Pitz, J.P. Vernon, Composite Structures **322**, 117422 (2023). DOI https://doi.org/10.1016/j.compstruct.2023.117422. URL https://www.sciencedirect.com/science/article/pii/S0263822323007687
19. J. Mackenzie, Proceedings of the Physical Society. Section B **63**(1), 2 (1950)